Title	Novel Plasma Generators for Advanced Thermal Processing
Author(s)	Kobayashi, Akira; Puric, Jagos
Citation	Transactions of JWRI. 2008, 37(2), p. 1-17
Version Type	VoR
URL	https://doi.org/10.18910/10465
rights	
Note	

Novel Plasma Generators for Advanced Thermal Processing[†]

KOBAYASHI Akira* and PURIC Jagos**

Abstract

Material processing using nano-technology is now advancing towards a more precise and controllable smart stage. Regarding thermal processing, the plasma system with high precise, has been proposed for advanced thermal processing. The gas tunnel type plasma system developed by the author exhibits high energy density and also high efficiency. Among its various applications is the plasma spraying of ceramics such as Al_2O_3 and ZrO_2. The characteristics of these ceramic coatings are superior to conventional ones. Another type of plasma generator is the high speed plasma accelerator developed at the University of Belgrade. It is operated in a low vacuum condition or with residual gas at low and high pressures. These systems are capable of generating high energy plasma flows of required composition within a large range of plasma parameters. Therefore this type of plasma accelerator will be also expected to be useful for advanced materials processing. In this paper, at first, the various types of plasma accelerators are described: Magnetoplasma Compressor of Compact Geometry (MPC-CG); MPC-Yu type; one stage Erosive Plasma Dynamic system (EPDS) and double stage Quasi-Stationary High Current Plasma Accelerator (QHPA) (in final stage of construction). The plasma flow produced by MPC-CG was used to investigate plasma flow interaction with solid silicon surfaces. Different types of submicron structure were obtained. Regarding the gas tunnel type plasma system, the performance such as the mechanical properties, thermal behavior and high temperature oxidation resistance of the alumina/zirconia functionally graded TBCs produced by spraying are described and discussed. The ZrO_2 composite coating has the possibility for the development of high functionally graded TBC (thermal barrier coating). The results showed that the alumina/zirconia composite system exhibited an improvement of mechanical properties and oxidation resistance. Also tungsten coating was introduced as one of heat resistant materials. Another application of gas tunnel type plasma is for the surface modification of metals. For example TiN films were formed in a short time of 5 s. And, the thick TiN coatings were obtained by gas tunnel type plasma reactive spraying. In this paper, the emphasis is on the explanation of the concepts and the features of these plasma systems and a description of the applications to the thermal processing.

KEY WORDS: (Gas tunnel type plasma system), (Plasma accelerator), (Al_2O_3 and ZrO_2), (Thermal barrier coating: TBC), (Silicon solid), (Surface modification)

1. Introduction

Nano-science & technology is one of the most important scientific fields. In order to apply Nano-science & technology to Material Science, material processing should be developed towards more precise and controllable smart processing stages. Regarding an applicable heat source, an important key will be the performance of the applied heat source. A plasma is one of the most superior heat sources, because of high temperature, high energy density, ease of control, etc. Therefore more precise plasma systems have been sought in order to establish smart thermal processing.

The gas tunnel type plasma system developed by the author has high energy density and also high efficiency[1-3]. An outline of this plasma system and its application to various thermal processes are described briefly in the following chapters. One typical application is the plasma spraying of ceramics such as Al_2O_3 and ZrO_2[4]. The characteristics of these ceramic coatings by the gas tunnel type plasma spraying were superior to those by conventional jets. Usually, the Vickers hardness of this sprayed coating became 20-30% higher than that of conventional plasma sprayed coating. And, the porosity was only half of the value of the conventional ones [5].

Plasma sprayed zirconia coatings are widely used as thermal barrier coatings (TBC) for high temperature protection of metallic components in the hot section of gas turbine such as burners, transition ducts, vanes and blades. It allows high temperature operation and results in an increase in the efficiency of the engine and the durability of its critical components. Although zirconia coatings have been used in many applications, the interface spallation problem due to the interface oxidation[6] is still waiting to be solved under the extreme

---

conditions such as high temperature and high corrosion environments. For TBC, the spalling of the coating is also a very important problem as well as the coating quality.

There have been many investigations in the development of high quality TBCs for diesel engines [7-8]. It is reported that the spallation rate can be relatively reduced by using suitable bond coats for the interface[9]. Nevertheless, it is difficult to find suitable bonding layers for all kind of substrate material. Alumina / zirconia composite coating was proposed as a potential candidate to improve the properties of thermal barrier coating systems due to alumina's low melting point and high hardness. Also, extremely high porosity values (up to 25vol%) of TBC s have been obtained by functionally graded layers of alumina. TBC failure occurs easily at the interface between the metallic bondcoat and topcoat. During high temperature service an oxide scale consisting mainly of α-alumina forms along the bond/topcoat interface.

While the large porosity and the high melting point is an advantage of ZrO_2 coatings, the porosity has disadvantages for adoption under critical conditions such as high temperature and a high corrosion environment. The resistance for thermal shock and high temperature corrosion are important properties in the high performance TBC. New types plasma spray methods are expected to exploit the excellent characteristics of ceramics such as corrosion resistance, thermal resistance, and wear resistance[10] by reducing the porosity and increasing the coating density.

A high hardness ceramic coating could be obtained by the gas tunnel type plasma spraying, and was investigated in detail in the previous studies [5, 11-14]. The Vickers hardness of the zirconia (ZrO_2) coating was increased with decreasing spraying distance, and a higher Vickers hardness could be obtained at a shorter spraying distance. At L=30 mm, when P=33 kW, the Vickers hardness of ZrO_2 coating was about Hv=1200 [15], which corresponds to the hardness of sintered ZrO_2 (Hv＝1,300). The ZrO_2 coating formed had a high hardness layer at the surface side, which showed the graded functionality of hardness[16-18]. With an increase in the number of traverses during plasma spraying, the hardness distribution was much smoother, corresponding with the result that the coating became denser. For TBC, the spalling of the coating is also a very important problem as well as the coating quality[19]. Thus, one of the advanced plasma applications with smart coating technology is expected to produce the desired characteristics of ceramics with improved corrosion resistance, thermal resistance, and wear resistance.

Regarding the plasma accelerator, several experimental set-ups have been constructed for the investigation of different types of new generation quasi-stationary plasma dynamic accelerating systems. These systems are capable of generating high energy plasma flows of required composition within a large range of plasma parameters; working in two different regimes: in vacuum, or residual gas at low or high pressures.

Until now, the following plasma accelerators have been realized: Magnetoplasma Compressor of Compact Geometry (MPC-CG); MPC-Yu type; one stage Erosive Plasma Dynamic system (EPDS) and double stage Quasi-Stationary High Current Plasma Accelerator (QHPA) (in final stage of construction).

Plasma flow produced by MPC-CG was used to investigate plasma flow interaction with solid silicon surfaces. Different types of submicron structure have been obtained.

In this paper, at first, the various types of plasma accelerators are described: Magnetoplasma Compressor of Compact Geometry (MPC-CG); MPC-Yu type; one stage Erosive Plasma Dynamic system (EPDS) and double stage Quasi-Stationary High Current Plasma Accelerator (QHPA) (in final stage of construction).

Regarding the gas tunnel type plasma system, its merits for smart thermal processing are described and one typical application to plasma spraying of ceramics such as Al_2O_3 and ZrO_2 described. The mechanical properties, thermal behavior and high temperature oxidation resistance, of high hardness ZrO_2 composite coating are described and its merit as TBC (thermal barrier coating) is discussed. The effect of alumina Al_2O_3 mixing ratio on the Vickers hardness of the ZrO_2 composite coating is explained in order to develop high functionally graded TBC. Moreover the adhesive characteristics of such high hardness zirconia-alumina (ZrO_2-Al_2O_3) composite coatings are described. In addition, the tungsten coating by the gas tunnel type plasma spraying was described as one of heat resistant materials for nuclear reactor [20-21].

Another application of gas tunnel type plasma is for the surface modification of metals. For example TiN films of 10μm thickness are formed in a very short time of several seconds [22]. The properties of TiN films are described, and thick TiN coatings by the gas tunnel type plasma reactive spraying [23] are introduced. Finally, regarding other applications of high-energy plasma to thermal processing, the development of a new type of smart plasma system is also discussed.

2. Design, Development and Construction of New Type Plasma Accelerators

### 2.1 Kinds of plasma accelerators

Now, there are many type of Plasma Accelerators were developed at University of Belgrade until now. The kinds of Plasma Accelerators are listed in **Table 1**

These are: Magnetoplasma Compressor of Compact Geometry (MPC-CG); MPC-Yu type; one stage Erosive Plasma Dynamic system (EPDS) and double stage Quasi-Stationary High Current Plasma Accelerator (QHPA) (in final stage of construction).
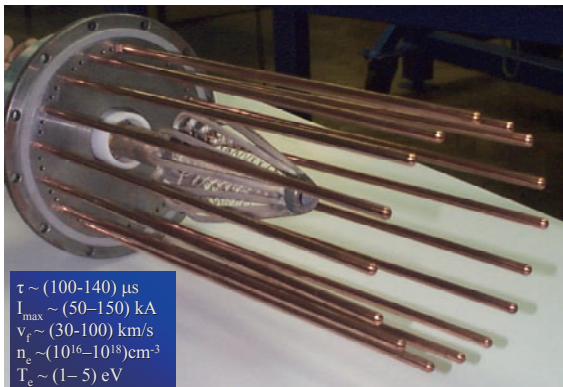
Figure 1 shows the image of the double stage Quasi-Stationary High Current Plasma Accelerator (QHPA) in **Fig.3** installed in the plasma vacuum chamber of 4m length.
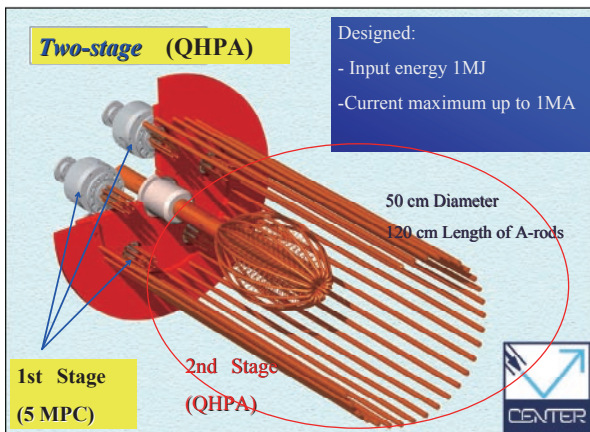
Table 1 Kinds of Plasma Accelerators.

- **Magnetoplasma Compressor (MPC)**
- **MPC Yu type**
  - one stage **Erosive Plasma Dynamic System (EPDS)**
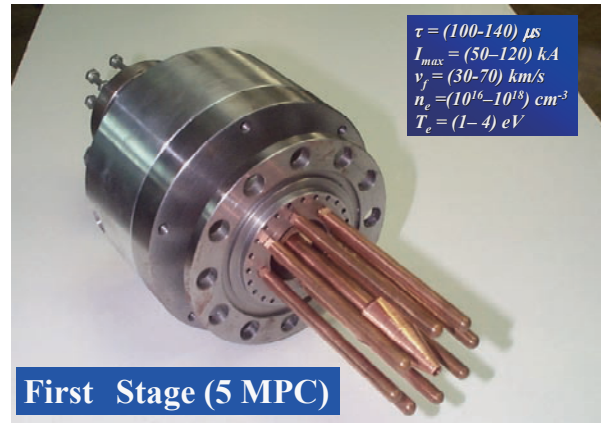 - two stage **Quasistationary High Current Plasma Accelerator (QHPA)**
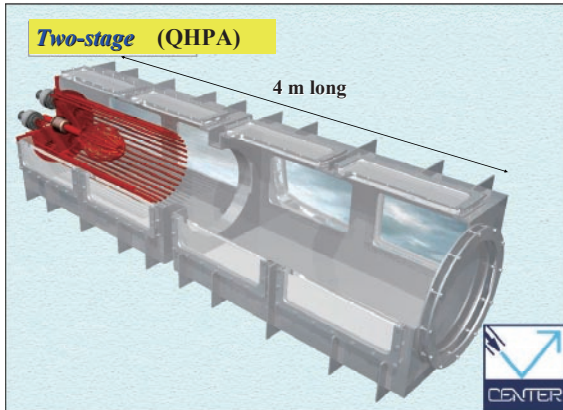
Fig.1 Double stage Quasi-Stationary High Current Plasma Accelerator (QHPA) in Fig.3 (in final stage of construction) installed in the 4m long chamber.

$\tau \sim (100\text{--}140) \ \mu s$
$I_{max} \sim (50\text{--}150) \ kA$
$v_f \sim (30\text{--}100) \ km/s$
$n_e \sim (10^{16}\text{--}10^{18}) cm^{-3}$
$T_e \sim (1\text{--}5) \ eV$

Fig.2 MPC-Yu type Plasma Accelerator.

Designed:
- Input energy 1MJ
- Current maximum up to 1MA

50 cm Diameter
120 cm Length of A-rods

1st Stage (5 MPC)
2nd Stage (QHPA)

Fig.3 double stage Quasi-Stationary High Current Plasma Accelerator (QHPA) (in final status of construction).

$\tau = (100\text{-}140) \ \mu s$
$I_{max} = (50\text{--}120) \ kA$
$v_f = (30\text{-}70) \ km/s$
$n_e = (10^{16}\text{--}10^{18}) \ cm^{-3}$
$T_e = (1\text{--} 4) \ eV$

First Stage (5 MPC)

Fig.4 Magnetoplasma Compressor of Compact Geometry (MPC-CG) Anode rods 14 cm in length, 0.8cm in diameter, Anode diameter 5 cm.

Figure 2 shows the photograph of MPC-Yu type Plasma Accelerator.

Figure 3 illustrates the double stage Quasi-Stationary High Current Plasma Accelerator (QHPA) in final stage of construction. And **Figure 4** is the photograph of Magnetoplasma Compressor of Compact Geometry (MPC-CG), which is used as the first stage of QHPA sown in Fig.3.

2.2 Investigation of the performance of main plasma accelerator properties (MPC)

The plasma Accelerator Properties (MPC) in Fig.4 were investigated and the following plasma parameters were defined. They are, Discharge duration τ, Flow velocity vf, Electron temperature Te, Plasma density n e, and also Minimal electrode erosion.

The methods are as follows:

(1) Spectroscopic investigations of compression plasma flows (CPF) generated by gas-discharge and erosive magneto plasma compressors

(2) The spatially- and time-resolved measurements of temperature and electron concentration of compression plasma flow in such quasi-stationary plasma accelerators

To characterize the quasi-stationary plasma flow, special dynamic coefficients were introduced in this study. These coefficients are calculated on the basis of the obtained temporal evolution of the plasma electron density and temperature, and discharge current.

In these experiments we have used a magnetoplasma compressor, a plasma source first designed, developed and investigated by group led by Prof. Morozov [24]. This plasma accelerator (plasma gun) is a source of quasistationary compression plasma flow.

In this case, the Anode rods were 14 cm in length, 0.8cm in diameter, Anode diameter 5 cm, respectively.

The Main Parameters of Magnetoplasma Compressor (MPC) are shown in **Table 2**.

Table 2 Main Parameters of Magnetoplasma Compressor (MPC).

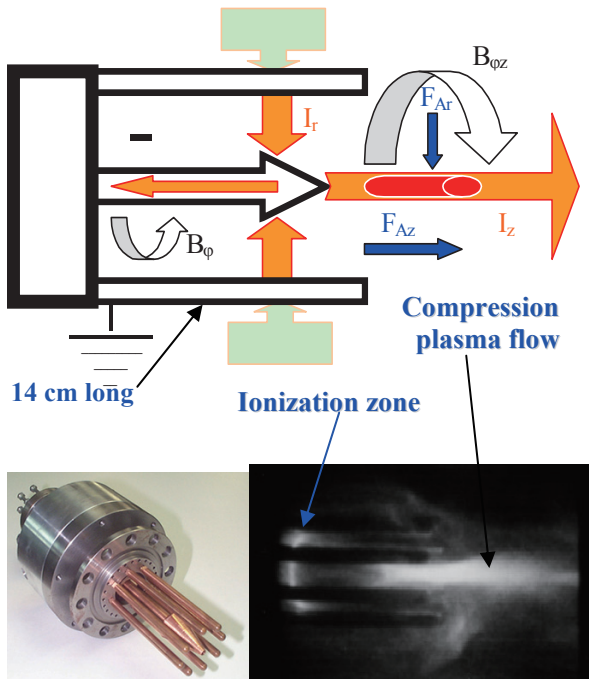| |
|---|
| $\tau = (100\text{-}140)\ \mu s$ |
| $I_{max} = (50\text{–}120)\ kA$ |
| $v_f = (30\text{-}70)\ km/s$ |
| $n_e = (10^{16}\text{–}10^{18})\ cm^{-3}$ |
| $T_e = (1\text{–}4)\ eV$ |

2.3 Principle scheme of MPC

Figure 5 shows the illustration of the concept of MPC. As an energy source a capacitor bank of 800 μ F, 4 kV was used, and for a typical condition, the working gas (nitrogen at 400 Pa pressure) was supplied in the torch backside. Plasma was generated at the ionized zone and flowed out from the torch. The plasma was magnetically compressed and accelerated, to form a Compression Plasma Flow (CPF) at ultra-high speed.

In this case, the main characteristics of the CPF are as follows [25-26]:
- the maximum discharge current of 70 kA
- 50 μ s long CPF steady state
- size: up to 6 cm in length and 1 cm in diameter
- flow velocity 40 km/s (in hydrogen ~100 km/s)
- electron density up to 4·1017 cm-3
- electron temperature up to 2-3 eV

Figure 6 shows the electrical and energy discharge parameters for MPC operating in nitrogen at 400 Pa pressure. Fig.6 (a) is the current and voltage oscilloscope traces; (b) is the discharge volt-ampere characteristic, (c)

is the time dependence of instantaneous power, and (d) is also the time dependence of energy. The current was the maximum value of 70kA at 20 μs, but the instantaneous power was increased till 40 μs. This means the input power to the plasma would be increased till 40 μs as is shown in Fig. 6(c). The plasma energy would be a maximum at 40 μs.

Figure 7 shows the Discharge volt-ampere characteristics for different working gases (Ar, N$_2$ and H$_2$). The discharge voltage increased with an increase in the current. And the voltage was lowest in the case of Ar, on the other hand H$_2$ was highest because of its high ionization voltage.

Now , Morozov A was introduced the Volt-ampere curve exponents α [24] as the functions of pressure.

$$U \sim I^3 \cdot \dot{m}^{-1} \tag{1}$$
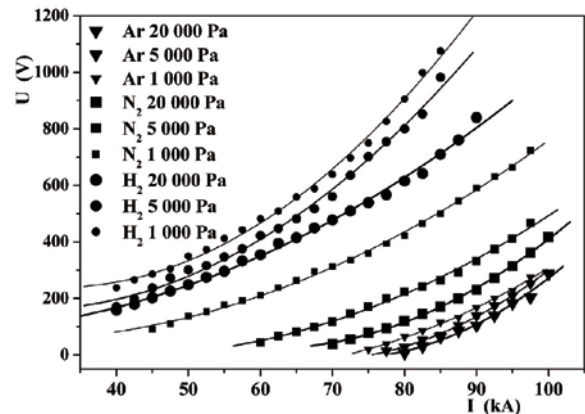
Here, U is discharge voltage, I: current, and m: mass flow rate.
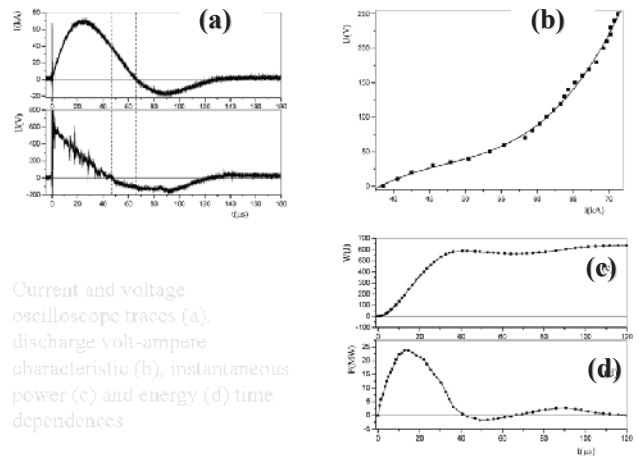
Fig.6 Electrical and energy discharge parameters. Current and voltage oscilloscope traces (a), discharge volt-ampere characteristic (b), instantaneous power (c) and energy (d) time dependences

Fig.5 Principle scheme of MPC the illustration of the concept of MPC.

Fig.7 Discharge volt-ampere characteristics for different working gases (Ar, N$_2$ and H$_2$)

In the experiments, we introduced the new Volt-ampere curve exponents α as

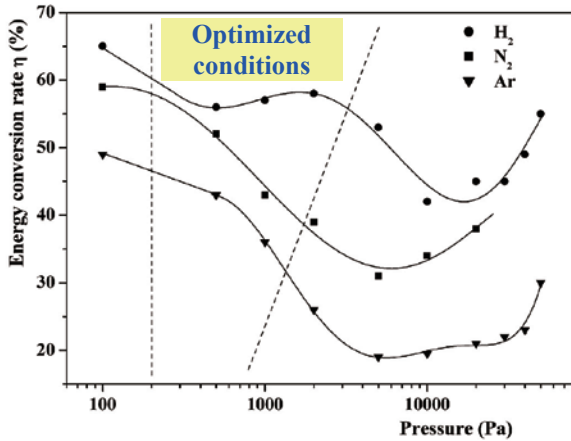$$U \sim I^{\alpha} \tag{2}$$

Fig.8 Pressure dependences of the energy conversion rate for different gases (U0 = 4 kV).
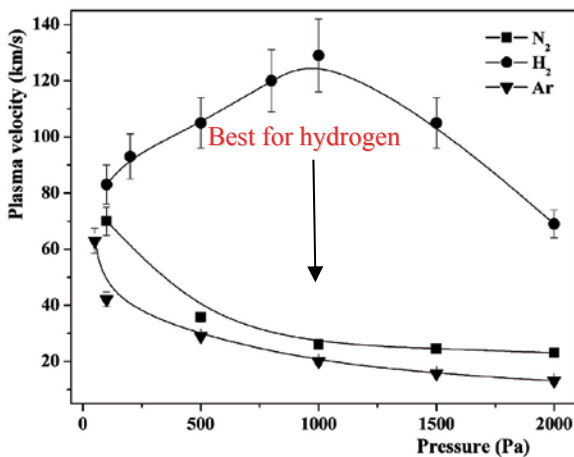

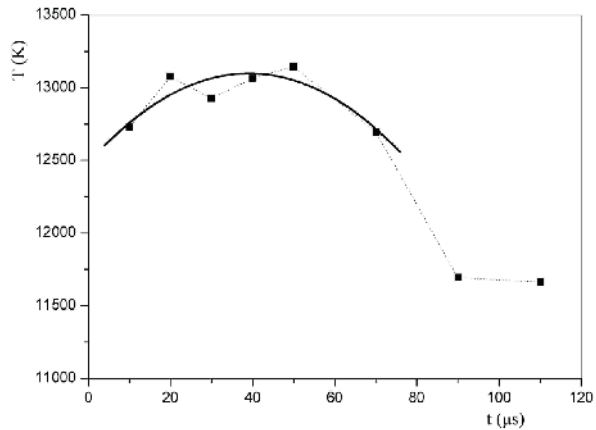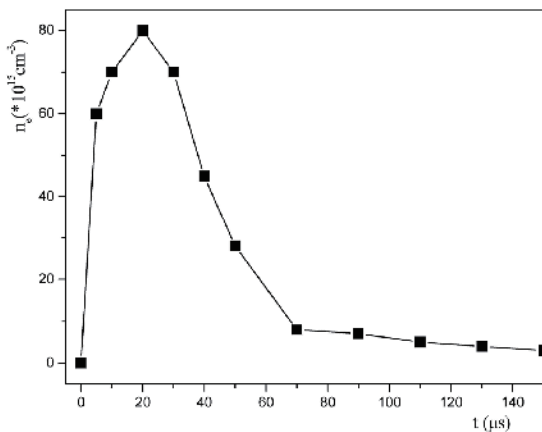**Fig.9** Pressure dependences of Plasma velosity for different gases.

The Volt-ampere curve exponents α for different working gases as the functions of pressure for different working gases. In the case of Hydrogen, Volt-ampere curve exponents α was the amount between 2-3, and maximum of 2.7 at 1000 Mpa. For pressure below 2000MPa, in a nitrogen discharge it has a similar value to α in Hydrogen.

Figure 8 shows the pressure dependences of the energy conversion rate for different gases (Ar, N_2 and H_2) at U0 = 4 kV. The pressure ranges appropriate for plasma accelerating working regimes in MPC are shown with dashed lines. The pressure range of the optimized condition was 200-3000 MPa for Hydrogen. And the energy conversion rate was 55-60% for H_2.

Plasma flow velocity for different working gases as functions of pressure (6.4 kJ supply energy) are shown in **Fig.9**.

Plasma flow velocity had maximum value for hydrogen only at the pressure range of the optimized condition. The maximum value of Plasma flow velocity was 130 km/s at 1000 Pa.

Thus, the most effective energy transfer from power supply to plasma is in hydrogen as a working gas at ~1000 Pa pressure. The maximum values of plasma flow velocities are obtained in hydrogen at this pressure (~130 Km/s). This is in accordance with the maximum value of the volt-ampere curve exponent obtained for MPC when operating in hydrogen (~2.7).

In argon and nitrogen the accelerating regime is violated when MPC is operating at pressures larger than 1000 Pa and 2000 Pa, respectively. (Fig.8, 9) For pressures larger than these the conditions for a decelerating regime are fulfilled.

For the pressures of the order of 100 Pa the influence of the eroded material from the cathode is predominant. Spectra were obtained by end-on observation in H_2 at different pressures (6.4 kJ): 10 000Pa, 1000 Pa and 100 Pa. And the Cu lines from the cathode were observed clearly as compared with H Balmer lines, which were increased with an increase in the pressure. In this case the

Fig.10 The electron density and electron temperature time dependences (Ar+3% H_2, 800 µF, 3.5 kV).

plasma flow velocities and volt-ampere characteristics are approximately the same in all working gases.

Also, the Balmer alpha line from side-on observation in H_2 was investigated at different times in order to decide the plasma flow parameters: electron density and electron temperature [27].

Figure 10 shows the time dependences of electron density and electron temperature at Ar+3% H_2 mixture, 800 μF, 3.5 kV. The parameters were derived by the measurement of the Balmer alpha line. **Fig.10 (a)** is the time dependence of electron density: ne. The electron density was maximum value of ne $=8 \times 10^{16}$ cm-3 at 20 μs. This time corresponded to the time when the discharge current had its maximum value. The electron density was decreased after 20s and became a very low value at more than 60s.

And **Fig.10 (b)** shows the time dependence of electron temperature Te. The electron temperature was Te = 13 200 K during 20-50s.

The spatial distributions of plasma parameters were measured. The time dependences of axial distributions of Balmer alpha line intensity, observed from side-on in H_2 plasma, showed that the plasma was uniform between the torch exit and 4.0 cm from the torch at the time of 20 μs.

Figure 11 shows the Electron density time dependences from side-on observation in H_2 with one high speed camera frame. The electron density was calculated by the Balmer alpha lines, therefore it was uniform distribution at the time of 20 μs. The uniform range of n_e $=3 \times 10^{17}$ cm-3 was about 30 mm. The uniform distribution gradually decayed as time was increased.
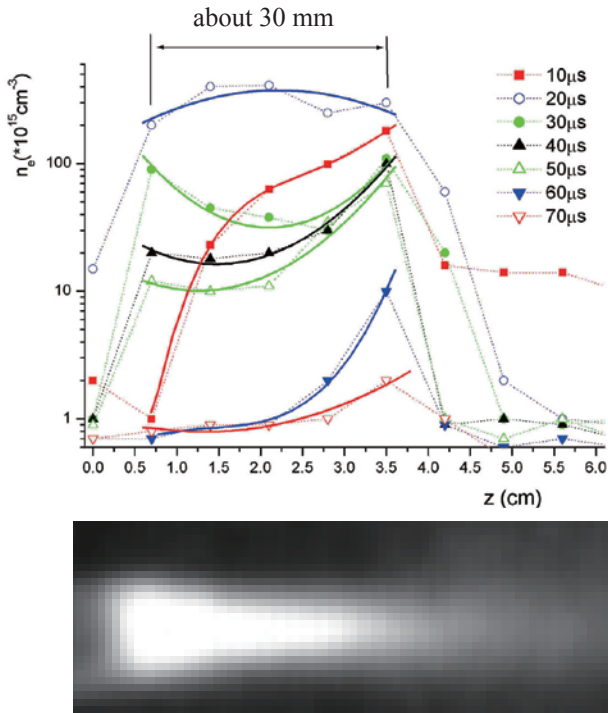
Intensities of: a) Hα, Hβ and Hγ; b) ArI 696.5 nm, Ar II 480.6 nm spectral lines versus time compared with continuum radiation intensity and discharge current time evolutions [28].

3. Applications of Plasma Accelerator

Here we introduce two types of plasma accelerator applications.

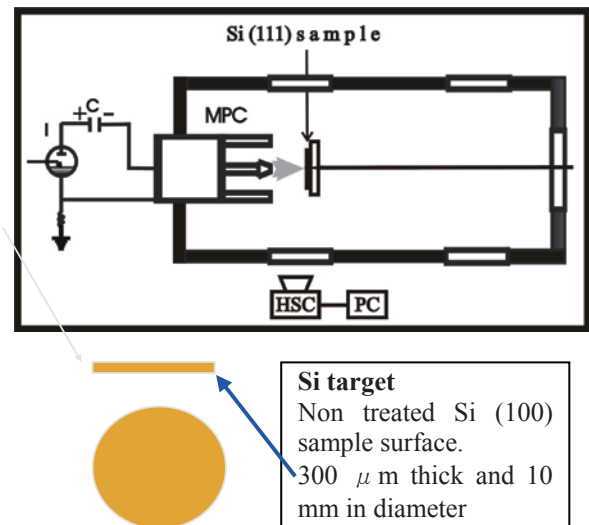One is the creation of submicron highly oriented structures on silicon single crystals.

Another is that using plasma flow from MPC, a silicon monocrystal surface was treated and different forms of submicron structures were found: from nanowires to nanodots.

Figure 12 shows the schematic diagram of the experiment using MPC. The samples were glued to the cylindrical brass holder of the same diameter with conductive carbon paste, and mounted perpendicularly in front of the MPC cathode at the distance of 5 cm. The target surface is parallel to the direction of gravitation force and perpendicular to the plasma flow velocity.
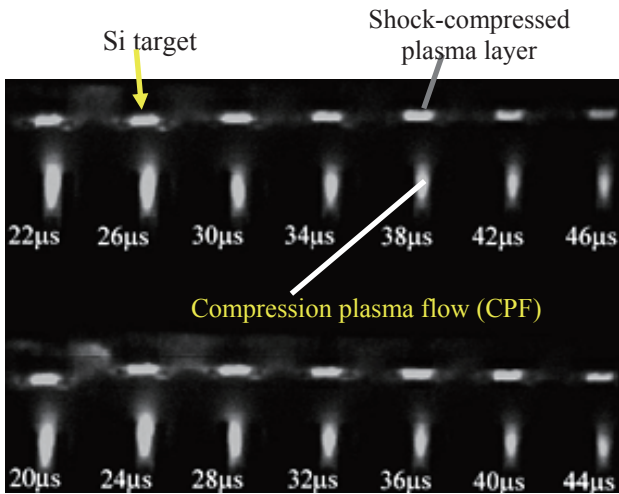
3.1 Interaction of CPF with silicon single crystal surface

For the studies of the CPF interaction with silicon surfaces, one-side polished n-type silicon wafers (100 orientation) 300 μm thick and 10 mm in diameter were used (See Fig.12).

Figure 13 shows the time evolution of plasma flow action of Si target. The interaction of CPF with the target causes the formation of a shock-compressed plasma layer (SCPL), and a plasma plume which results in the shielding of the target surface from direct action of a CPF. The thickness of the SCPL is about 1 cm.

Fig,11 Electron density time dependences from side-on observation in H_2 with one high speed camera frame.


Fig.12 Schematic diagram of experiment.

6

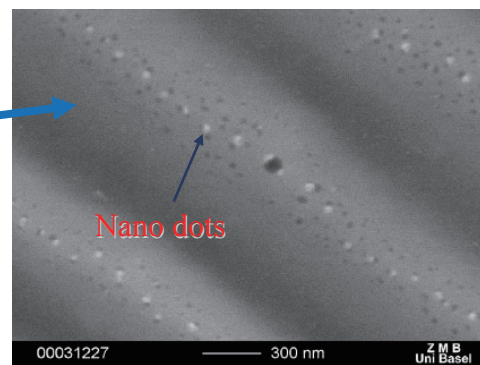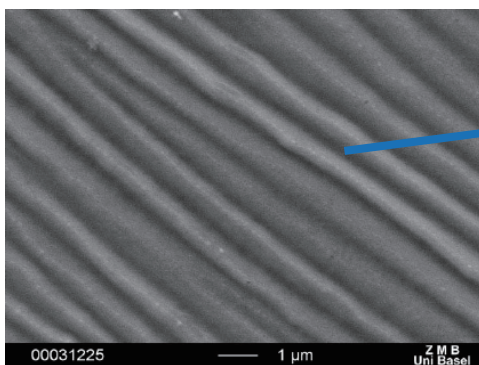**Fig.13** Time evolution of plasma flow action of Si target.

After the plasma processing (plasma flow action), silicon surface structures of a non treated Si (100) sample was changed to the shapes shown in **Fig. 14 and Fig.15**.

Figure 16 shows the surface transformation model after compression plasma flow action. Here the absorbed energy was 10-15 J per pulse, flow power density $\sim10^5$ W/cm^2. In this case, the shock-compressed plasma layer was estimated as (~1 cm), and the Molten layer on the target surface; ($\sim10\,\mu$ m).

The CPF kinetic energy thermalization caused the SCPL heat up. The CPF energetic action on the surface is causing the fast heating and melting of the surface layer. It may be taken that molten layer exists on the target surface during the interaction ($\sim50\;\mu$ s). Thickness of the near-surface molten layer is estimated at 6-10 μ m.
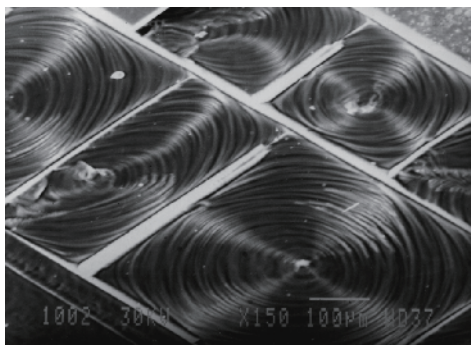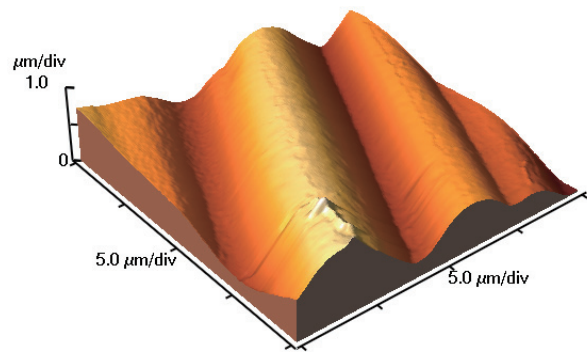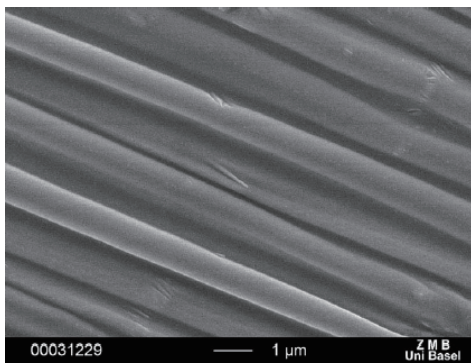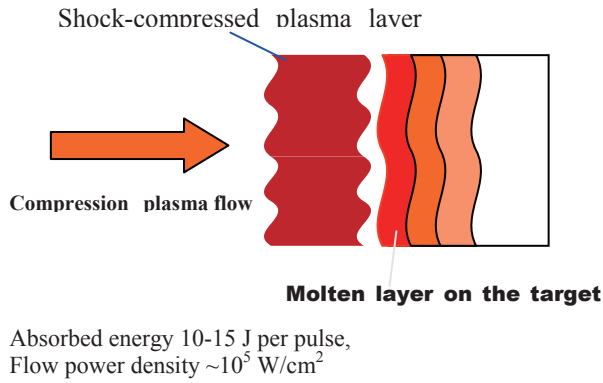

Fig.14 Silicon surface structures after plasma flow action (1).

Fig.15 Silicon surface structures after plasma flow action (2).

Shock-compressed plasma layer

Compression plasma flow

Molten layer on the target

Absorbed energy 10-15 J per pulse,
Flow power density $\sim 10^5$ W/cm^2

Fig.16 Surface transformation model after compression plasma flow action.

μ m/div
0.4

0

2 μ m/div

2 μ m/div

Fig.18 AFM micrograph of CPF treated Si (100) surface.

3.2 Capillary waves

If the free surface of a liquid is put out of balance, waves are formed along the surface under the influence of gravitational pull and surface tension. If the direction of the gravitation force is such that it can not contribute to the creation of surface waves, the waves formed at the liquid surface are capillary waves [29].
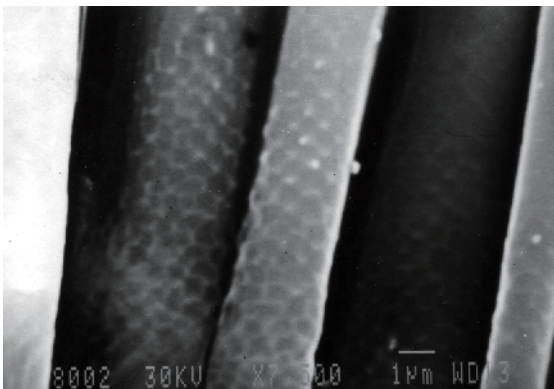
The dispersion of such capillary waves is given as:
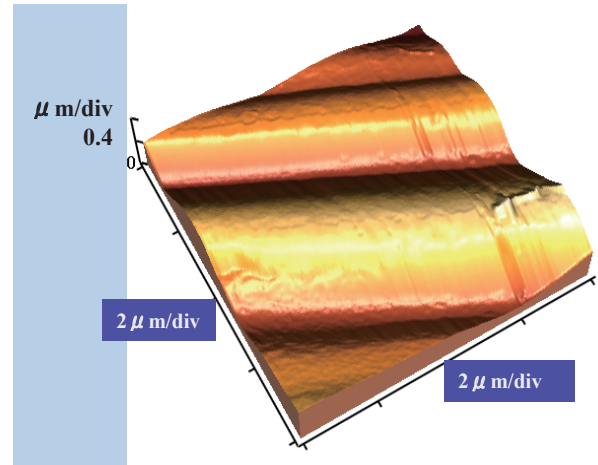
$$\omega^2 = \frac{\gamma}{\rho} k^3 \qquad (3)$$

Here, γ is the surface tension, ρ is the density of the liquid, ω is the frequency and k is wave number of the capillary waves.

3.3 Relation between treated surface and plasma structures of CPF

The time development of CPF was observed using a high speed camera operating in streak mode, using parallel positioned slits along the CPF axis. Discrete plasma structures of CPF, seen as light and dark regions, were observed. These structures occur with ~5 MHz

frequency. The compression plasma flow had intrinsic oscillations. The MPC forms discrete plasma structures of CPF with an intrinsic frequency.

Therefore, CPF treatment of the melted silicon surface is a periodical perturbation due to CPF intrinsic oscillations (~5 MHz frequency). **Figure 17** shows Silicon surface periodical cylindrical structures, which are **CPF induced capillary waves;** these corresponds to liquid surface structures frozen during fast cooling [30].

Figure 18 shows the AFM micrograph of a CPF treated Si (100) surface. The AFM micrographs were used for the periodical structures surface investigation. The periodical structures have a wavelength of about 4 μ m, and amplitude (half hill-to-valley distance) of 0.2 μ m.

4. Further Directions in Applications of Plasma Accelerators

These systems may have different application, such as:

- Obtaining materials with improved qualities due to the plasma flow interaction with solid surfaces;
- Coatings technology;
- Creation of nanostructures (silicon single crystals)
- Quasistationary high-current plasma accelerator (QHPA) as plasma injector for fusion devices.
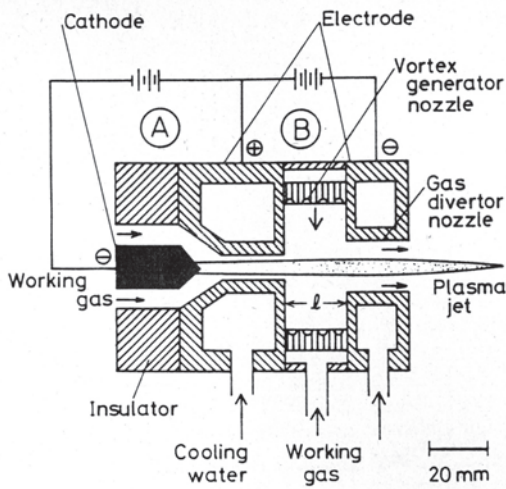
We are considering the possibility of the Joint Research Program for studying the plasma flow interaction with material coatings such as ZrO_2, Al_2O_3, SiO2, W, DLC, and their composites, obtained using a novel gas tunnel type plasma source developed at JWRI.
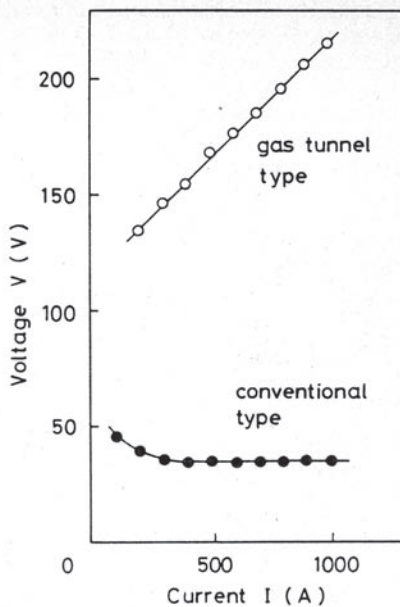
5. Gas Tunnel Type Plasma System

The schematic of gas tunnel type plasma torch developed by the author is shown in **Figure 19**. The working gas makes a strong vortex flow in the chamber, and forms a low pressure gas tunnel along the torch

Fig.17 Silicon surface periodical cylindrical structures by CPF (compression plasma flow) action.

center axis. This makes plasma production easier, and the strong vortex constricts and stabilizes the plasma jet. **Figure 20** shows the current-voltage characteristic of this gas tunnel type plasma jet. The gas tunnel type plasma jet is high voltage type and also has a positive current-voltage characteristic, while the conventional one has a negative characteristic.

The comparison of the shape of plasma jet is shown in **Fig.21**. The gas tunnel type plasma jet is longer and more stable than the conventional ones. **Table 3** shows the feature of gas tunnel type plasma jet as compared to the conventional ones. The gas tunnel type plasma system has high energy density and also high efficiency[1-3].

One example of application of the gas tunnel type plasma is in thermal spraying. **Figure 22** shows the gas tunnel type plasma spraying torch. The behavior of the gas tunnel type plasma spraying is shown in **Fig.23**. This is the case of the deposition of Al_2O_3 powder. The experimental method to produce the high hardness ceramic coatings by means of the gas tunnel type plasma spraying has been described in previous papers[4-5,11-13].

Fig.19 Schematic of the gas tunnel type plasma torch.

Fig.20 Current-Voltage characteristic of Schematic of gas tunnel type plasma jet.
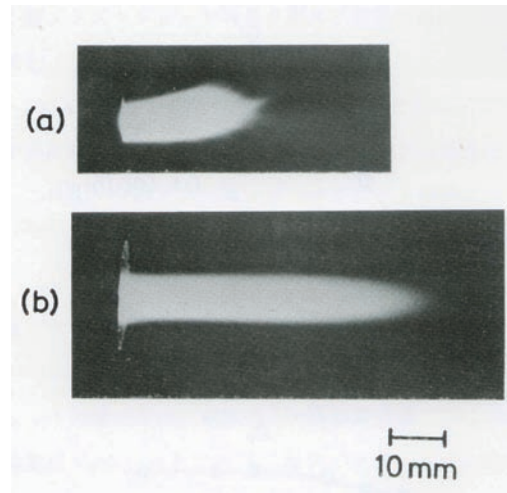
Fig.21 Comparison of the shape of plasma jet (500A).
 (a) conventional type plasma jet
 (b) gas tunnel type plasma jet (long, stable)

Table 3 Comparison between gas tunnel type plasma jet and conventional ones.

	Gas tunnel type plasma jet	conventional ones
Temperature	15000 K	10000 K
Energy density	10^5 W/cm^2	10^4 W/cm^2
Heat efficiency	80%	50%
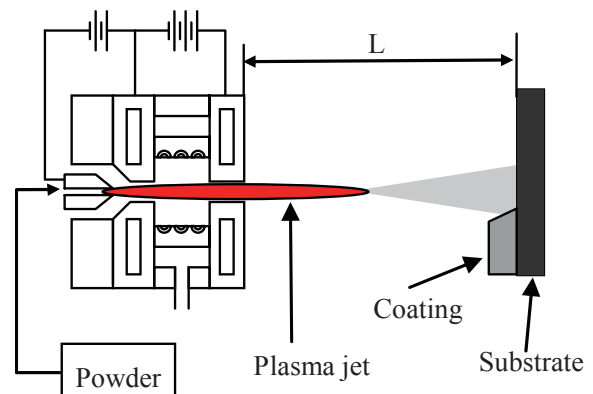
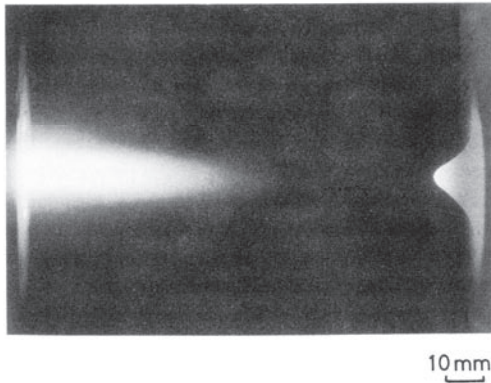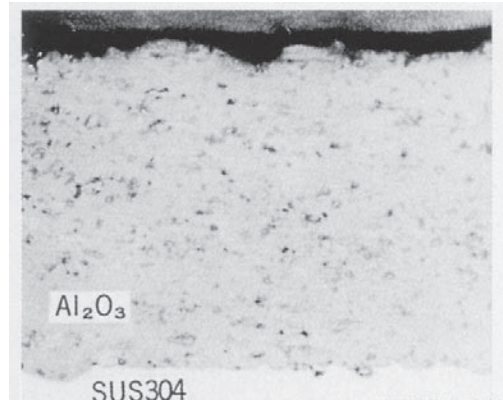Fig.22 Schematic of the gas tunnel type plasma spraying torch. *L*: Spraying distance.

Fig.23 Behavior gas tunnel type plasma spraying in. the case of deposition of Al₂O₃ powder. Spraying distance: 10cm.

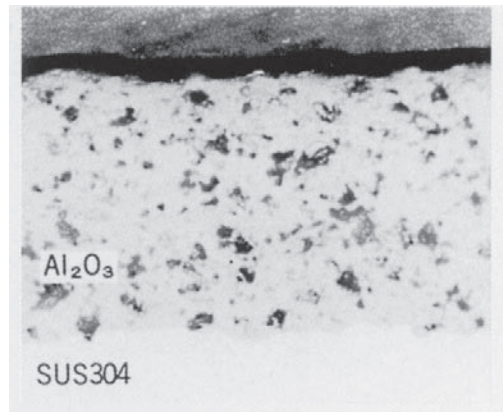(a) gas tunnel type plasma spraying

(b) conventional type.

Fig.24 Comparison of the cross section of alumina coating between gas tunnel type plasma spraying (a) and conventional type (b).

6. Gas Tunnel Type Plasma Spraying

The spraying powder is fed inside plasma flame in an axial direction from the center electrode of the plasma gun. So, the spraying powder becomes molten in the plasma, and plasma spraying for high melting point ceramics is available. The coating is formed on the substrate traversed at the spraying distance: L. In this case, the gas divertor nozzle diameter was d=20 mm.

This plasma system has many possibilities for industrial applications to the various thermal processing, such as plasma spraying, surface modification etc. The typical applications are:
1) Plasma spraying of ceramics (Al₂O₃ and ZrO₂ etc.)
2) Surface modification of Ti materials (Nitridation)
3) Other Applications such as nano-science, functional materials processing technology
4) Application to environmental problems, others.

Moreover, the development of new type of smart plasma system is planned in order to apply to thermal processing of materials and the environmental problems and so on.

6.1 Characteristics of gas tunnel type plasma spraying

The gas tunnel type plasma spraying can make high quality ceramic coatings compared to other plasma spraying methods. **Figure 24** is the comparison of the cross section of an Al₂O₃ coating by gas tunnel type

Table 4 Comparison between gas tunnel type plasma spraying and conventional type for Al₂O₃ coating. (Input ＝45kW、Distance = 65-100mm)

	Gas tunnel type plasma spraying	*Conventional ones*
Vickers hardness	1200	800
Porosity	10%	20%

plasma spraying and by a conventional method. The cross section of the coating by gas tunnel type plasma spraying is much denser. **Table 4** shows the quality (hardness, porosity, etc.) of the Al₂O₃ coating by gas tunnel type plasma spraying [11-13]. The hardness was like sintered alumina: Hv＝1,200 and high density, porosity was half of the value of the conventional ones. Even when the working gas is argon and with a low input of 20 kW, we can obtain a high Vickers hardness of Hv=800.

Thus it can be easy to produce the high hardness ceramic coatings by means of the gas tunnel type plasma spraying.

6.2 Experimental procedure

The gas tunnel type plasma spraying torch used was shown in Fig.22. The experimental method to produce the ceramic coatings by means of the gas tunnel type plasma spraying is as follows. After igniting the plasma gun, the main vortex plasma jet is produced in the low pressure gas tunnel. The spraying powder is fed from

Table 5 Experimental conditions.

Powder:	$ZrO_2 + Al_2O_3$ Mixture
Traverse number: N	1~30
Power input, P (kW):	25~28
Working gas	
flow rate, Q (l/min):	180
Powder feed gas, Q feed (l/min):	10
Spraying distance, L (mm):	40
Traverse speed, v (cm/min):	25~1000
Powder feed rate: w (g/min):	20~35
Gas divertor nozzle dia., d (mm)	20

Table 6 Chemical composition and size of zirconia and alumina powder used. （20~80% Al_2O_3 Mixture）

	Composition (wt%)					Size (μm)
ZrO_2	ZrO_2	Y_2O_3	Al_2O_3	SiO_2	Fe_2O_3	
	90.78	8.15	0.38	0.20	0.11	10-44
Al_2O_3	Al_2O_3	Na_2O	SiO_2	Fe_2O_3		
	99.8	0.146	0.01	0.01		10-35

the center inlet of the plasma gun. The coating is formed on the substrate traversed at the spraying distance of L.

The experimental conditions for the plasma spraying are shown in **Table 5**. The power input to the plasma torch was about P=25 kW, and the power input to the pilot plasma torch, which was supplied by the power supply PS-1, was turned off after starting. The spraying distance was short L= 40 mm.

The working gas was Ar gas, and the flow rate for the gas tunnel type plasma spraying torch was Q=180 l/min, and gas flow rate of the carrier gas was 10 l/min. The powder feed rate of zirconia/alumina mixed powder was w=20~35g /min. The traverse speed of the substrate was varied in value from v=25 to 1000 cm/min. Also the traverse number was changed 1-30 times. The thickness of the coating was 50~250μm. Also, the high speed traverse of v=1000cm/min, was repeated 30times.

The chemical composition and the particle size of Zirconia (ZrO_2) and/or alumina (Al_2O_3) powder used in this study are shown in **Table 6**. This ZrO_2 powder was the commercially prepared type of K-90 (PSZ of 8% Y_2O_3), and Al_2O_3 powder was the type of K-16T. The substrate was SUS304 stainless steel (3x50x50), which was sand-blasted before use.

The Vickers hardness Hv_{50}, Hv_{100} of the sprayed coatings was measured at the non-pore region in the cross sections under the condition that the load weight was 50g, 100 g and its load time was 25s. The Vickers hardness: Hv_{100} was calculated as a mean value of 10 point measurements. The distribution of the Vickers hardness in the cross section of the coating was measured at each distance from the coating surface in the thickness

direction. The microstructure of the cross section of zirconia composite coating was observed by an optical microscope.

The adhesive strength between the ZrO_2 composite coating and the substrate was measured by using the tension tester originally designed. The test piece for adhesive strength was 10mm square and the coating surface side and substrate side were respectively attached to each holder by polymer type glue. The load for the tester could be changed 0~200kg. The kgf/cm^2 was used as a unit for the adhesive strength of the composite coating. The adhesive strength of the ZrO_2 composite coatings was measured in the case of different coating thicknesses.
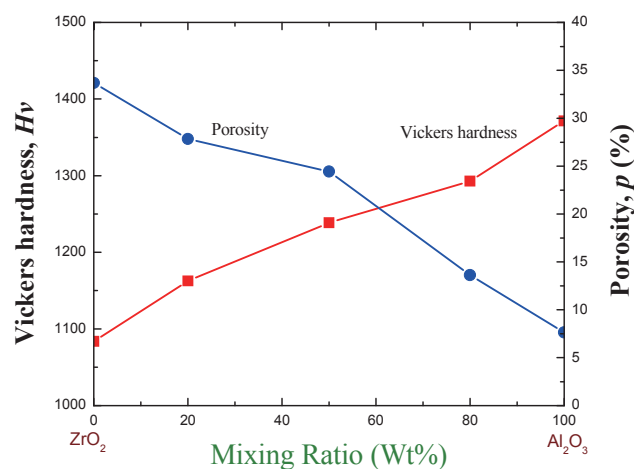
7. Zirconia Composite Coatings for TBC

7.1 Effect of the Alumina Mixing Ratio on Vickers Hardness of Zirconia Composite Coatings

Regarding the Vickers hardness on the cross section of ZrO_2 composite coating produced by the gas tunnel type plasma spraying for the same spraying time, the coating thickness was the same and the maximum Vickers hardness of the ZrO_2 composite coating was also same. But the graded functionality became much better with increasing the traverse number.

Figure 25 shows the dependence of Vickers hardness and porosity of ZrO_2 composite coatings, on the Al_2O_3 mixing ratio R(wt%). In this case, the coating thickness was approximately 200 μm at P=25 kW, L=40 mm, when the traverse number was two times.

The Vickers hardness of ZrO_2 composite coating increased with increases in the Al_2O_3-mixing ratio. The coating hardness corresponds to the high hardness of Al_2O_3 particles. Namely, the Vickers hardness of Al_2O_3 coating was Hv_{50}＝1440.


Fig.25 Dependence of Vickers hardness and porosity of zirconia composite coating on the alumina mixing rate. L=40mm when P=25kW.

11

The hardness distribution of the ZrO_2 composite coating has remarkable graded functionality in the case of large Al_2O_3 mixing ratios. The part near the substrate did not change so much, but the Vickers hardness near the coating surface became much higher. This leads to the development of a high functionally TBC.

7.2 Effect of High Speed Traverse on Coating Quality

For an increase in the traverse number, the surface temperature of the coating during spraying became higher. Therefore it would be expected that coating density would increase when the traverse number increased [18].

Figure 26 is the cross section of composite coating produced by high speed traverses at $P = 25$ kW, $L = 40$ mm. Traverse times was 30 times. This speed:
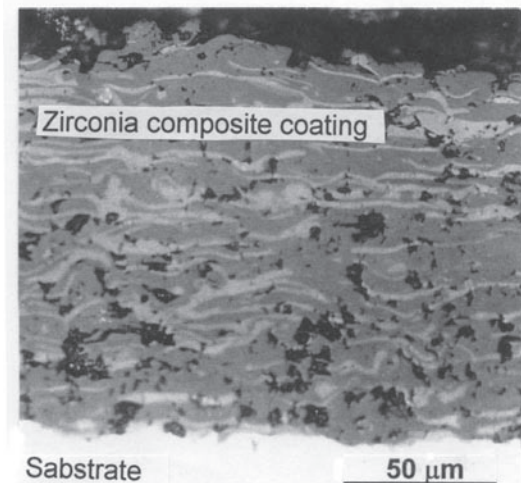
Fig.26 Microhotograph of cross section of zirconia composite coating. The traverse number was 30 time traverse. Sprayed at L=40mm when P=25 kW.
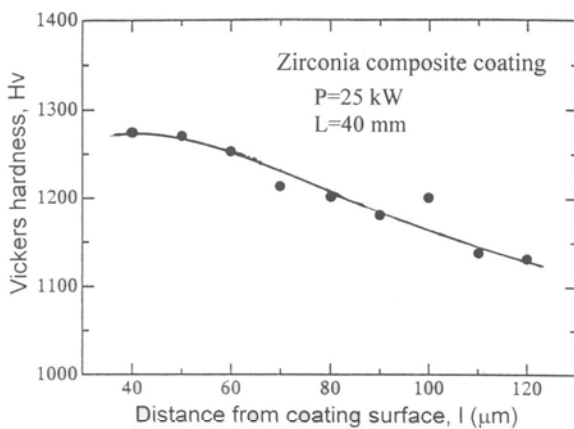
Fig.27 Surface morphology of the zirconia/alumina composite coating.

1000cm/min was 10 times higher than the normal speed traverse as in Fig.22. The thickness was about 150μm. It consisted of 2 different layers, white and gray layers were deposited alternately. The analysis by EPMA revealed that white is zirconia (ZrO_2) and gray is alumina (Al_2O_3).

The white ZrO_2 layer was a flat splat of uniform thickness, and embedded parallel in the Al_2O_3 matrix of low melting temperature. The black parts in the coating are pores, and are distributed through the whole coating. The surface side has fewer pores compared to the coating near the substrate and the structure is denser towards the surface of the coating.

Figure 27 shows the distribution of Vickers hardness: Hv_{50} of the zirconia/alumina composite coating shown in Fig.26 (coating thickness: about 150μm). Here, the left side axis is the surface of the coating. The distribution of this composite coating has a highest value in the coating at the surface side: The maximum hardness was near to $Hv_{50} = 1300$ at the distance from the coating surface of l=40 μm, and decreased linearly towards the substrate side.

Regarding the effect of traverse number, the uniformity of pores was improved and the deviation of hardness distribution was decreased. Therefore, the high speed and high number traverse improved the grade functionality of coating hardness. This shows the possibility of high performance TBC by high speed traverse processing.

7.3 Influence of Plasma Thermal Process on Coating Quality

The maximum Vickers hardness of the ZrO_2 composite coating was almost the same when the coating thickness was the same. But the graded functionality became much better, and the distribution of Vickers hardness was much smoother as the traverse number increased. This means that the structure at the surface of the coating was denser by the thermal process of the high energy plasma. **Figure 28** shows SEM photograph of the surface of the zirconia/alumina composite coating. It shows that the surface is formed by the mechanical interlocking at Al_2O_3 and ZrO_2 interfaces, and the higher surface roughness of alumina resulted in higher bond strengths

Regarding the microphotograph of ZrO_2/Al_2O_3 coating produced by the gas tunnel spraying on the fixed substrate for 3s spraying time, the coating thickness was about 250 μm, and white and gray layers were deposited alternately as shown in **Fig.29**.
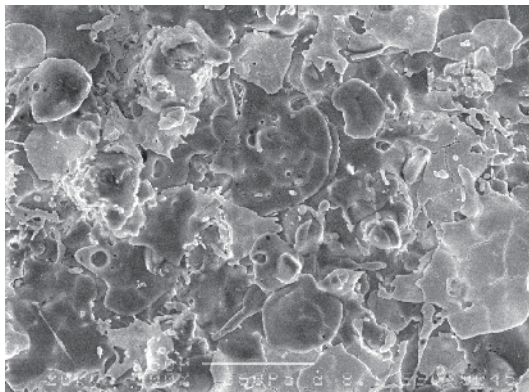
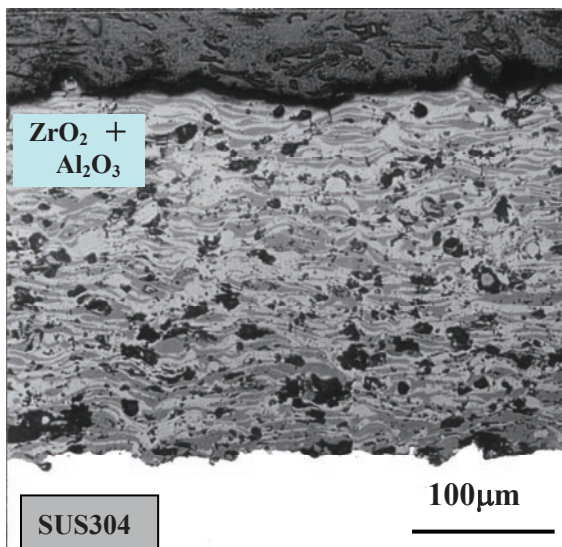**Fig.28** Surface morphology of the zirconia/alumina composite coating.

Fig.29 Typical ZrO_2/Al_2O_3 coating produced by the gas tunnel spraying on the fixed substrate for 3s spraying time.

The graded functionality of the structure is remarkable, and small pores are distributed disparately in the whole coating while larger pores exist near the substrate. The surface side has fewer pores and is dense, compared to the coating near the substrate. This was caused by the thermal process of the high energy plasma from the surface side of the coating.

In this case, the Vickers hardness linearly decreased in the thickness direction towards the substrate side. The dense microstructure led to the suppression of the deviation of the hardness distribution. This coating will be useful for high performance TBC.

7.4 Adhesive Strength of ZrO_2 Composite Coatings

Figure 30 shows the dependences of adhesive strength of the ZrO_2 composite coatings on the coating
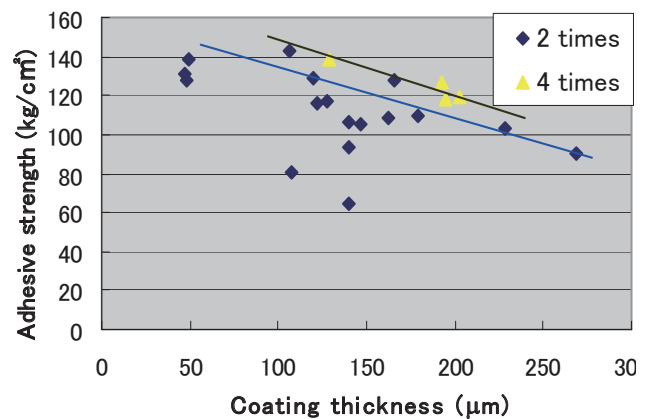

Fig.30 Adhesive strength of the ZrO_2 composite coatings vs. the coating thickness.

thickness. The adhesive strength of the ZrO_2 composite coatings decreased when the thickness was large. In the case of small coating thickness (100μm), the adhesive strength was large: it was more than 140 kgf/cm^2 for the coating thicknesses of below 100μm. The value was F = 100~120 kgf/cm^2 when the thickness was more than 200μm. Therefore the thick coating was much easier to break than the thin coating, but the adherence was improved when the traverse number was large.

8. Tungsten Coating for High Heat Resistant Materials

Tungsten (W) is a material which has the highest melting point of 3422 °C among metals. Therefore when deposited as a coating it can protect the substrate surface from high heat flux. The W composite will be a superior candidate of a material (such as TBC) for thermal fusion materials, etc. Pure tungsten coatings were sprayed onto stainless steel substrates using the gas tunnel type plasma spraying method. A thinner (~40 μm) tungsten coating was formed by traversing the substrate.

8.1 Experimental method for W coatings

The gas tunnel type plasma spray torch was shown schematically in Fig. 22. The experimental methods for production of the high hardness ceramic coatings by means of the gas tunnel type plasma spraying have been described in the previous publications [6-8].

The overall experimental conditions for the plasma spraying of tungsten are shown in **Table 7**. The input power to the plasma torch was about 22.5kW. A short spraying distance of L= 40 mm was chosen for all tungsten plasma spraying deposition processes. Argon was used as the working gas, and its flow rate was Q=170 l/min.

The powder feed rate of tungsten was about w=24 g/min and the gas flow rate of carrier gas was 10 l/min.

Table 7 Spraying condition for W coating.

Arc current	450A
Voltage	-50V
Spraying distance	40 mm
Working gas Ar flow rate	170 l/min
Feed gas flow rate	10 l/min
Powder feed rate	24 g/min
Traverse number	12 times
Spraying time	20 s

Table 8 The chemical composition and particle size of the tungsten powder used.
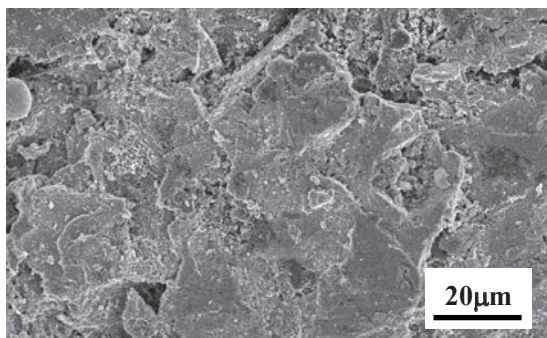
Material:	Tungsten (W)
Melting point:	$T_m = 3422^oC$
Purity:	99.9%
Particle size:	12 μm (average)

The substrate was traversed 12 times during the spraying. The chemical composition and particle size of the tungsten powder used are also given in **Table 8**. The tungsten powder was 99.9% in purity and the profile of the tungsten powder was not spherical, and the size is average 12 μm.
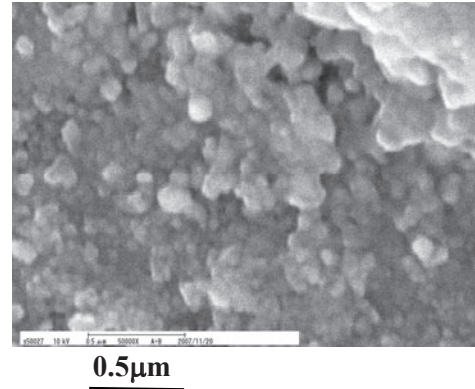
The cross section and surface morphology of the tungsten coatings was observed with an SEM to observe clearly the structure. X-ray diffraction (XRD) with a θ-2θ geometry was conducted for the crystal structure of the coatings utilizing a Co target and tube voltage of 30 kV and current of 14 mA. The Vickers micro-hardness of the sprayed tungsten coating was measured in cross sectional regions, where is free from porosity.

8.2 Microstructure of tungsten coating

Figure 31 shows the surface photograph of the tungsten coating sprayed at L=40mm with P=25 kW, taken by SEM. This photograph shows that tungsten powder was sufficiently molten. The length of each splat is more than 20 μm in this case. And there were nano

0.5μm

Fig.32 Surface of the coating appeared with nano particles taken by high magnification SEM. 27

W coating

40μm
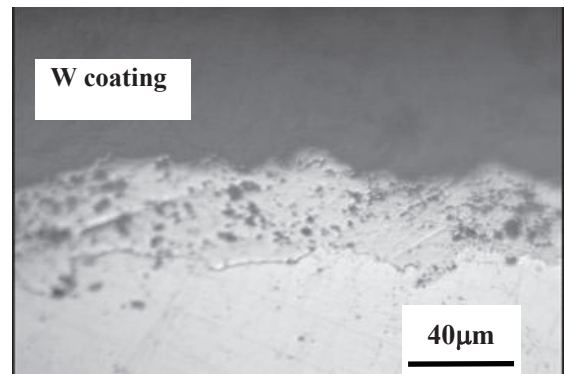
Fig.33 Cross-sectional optical microscope image of W coating sprayed at L=40mm with P = 25 kW.

size particles at some points on the coating surface (**Fig.32**). This means that there are some possibilities for the controllability of spraying condition in order to make nano size surfaces of W coatings in the future.

The cross section images of tungsten coating were taken by an optical microscope. **Figure 33** show the cross sectional image of the same tungsten coating samples as shown in Fig.31. The spraying time for this thin coating (~40μm) was 20s. The number of pores is substantially lower than that of zirconia coatings deposited under given conditions

8.3 Property of tungsten coating

Plasma sprayed pure tungsten coatings are black or grey in color. But generally yellow appears, which indicates the presence of tungsten oxides. In order to avoid oxidation, the sufficient argon gas flow must be supplied to keep the newly deposited tungsten under a shroud of inert gas, thus allowing it to cool quickly enough to avoid oxidation.

XRD measurement of the coating (40μm) is shown in **Fig.34**, which reveals several strong tungsten peaks and indicates the presence of pure tungsten phase. No tungsten oxide was observed by these XRD spectra
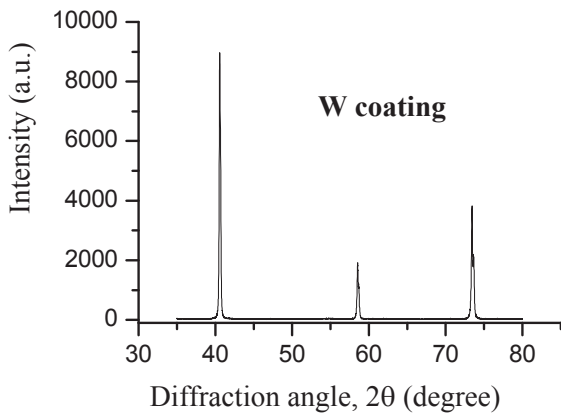

20μm

Fig.31 Surface photograph of the coating sprayed at L=40mm with P=25 kW, taken by SEM.

Fig.34 XRD pattern of the tungsten coating.

Fig.36 Concept of gas tunnel type plasma reactive spraying for TiN thick coating formation.

obtained. The absence of tungsten oxide peaks shows that only minimal oxidation occurred during the deposition processes. The result from XRD shows that the coating consists of pure metal tungsten.

The Vickers micro-hardness of the W coating was measured along cross section of each coating. The results showed that the Vickers micro-hardness of the thinner coatings was $Hv = 260$, which represents the average value for plasma sprayed tungsten coating. This Vickers micro-hardness was lower than that of pure bulk tungsten, which is about $Hv = 350$, probably because of the pores in the coatings.

9. Other Application of Smart Plasma System

Another application of the gas tunnel type plasma is surface modification of metals such as nitridation, carbonization, etc. For example the TiN films were formed in a very short time of 5 s by the irradiation of N_2 plasma jet as shown in **Fig.35**. The thickness of the TiN film was 10 μm and the film is of high quality (homogeneous and high density). The Vickers hardness was about 1700 on the cross section of the film [22].
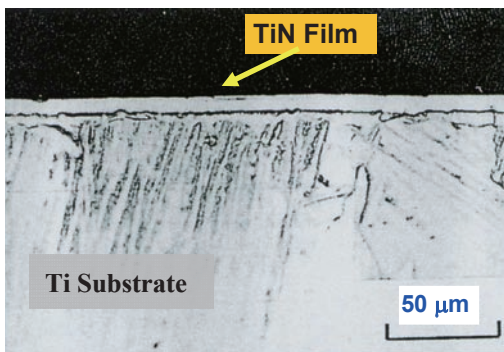

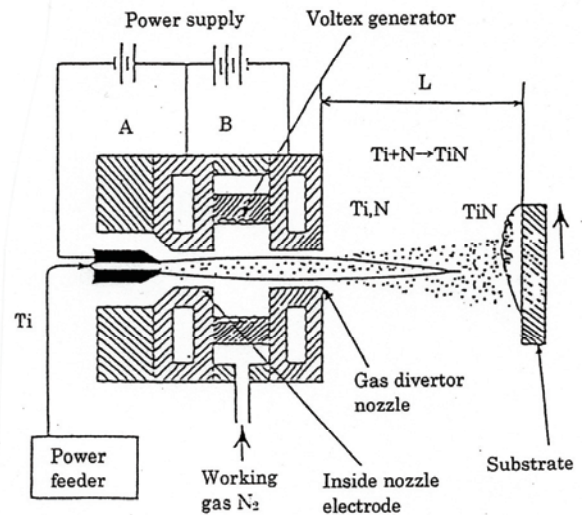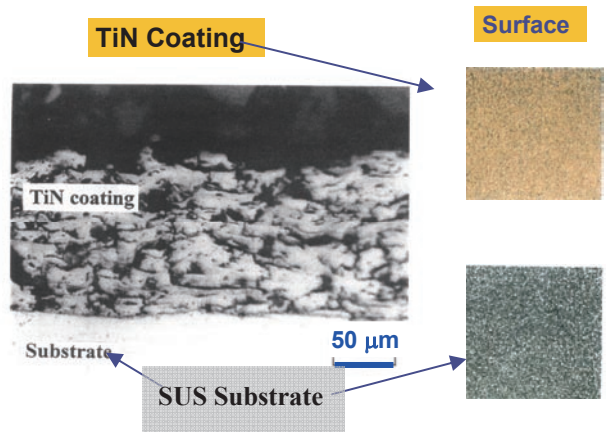Fig.35 Microhotograph of cross section of TiN film. Ti substrate irradiated at L=70mm when P=20 kW.

Fig.37 Cross section of typical TiN coating at P=25kW,、 L=60mm, t=5s and the surface view of the TiN coating (Hv=2000 and the substrate.

A new type of plasma reactive spraying was developed by using the gas tunnel type plasma spraying equipment. The thick TiN coatings were obtained by the gas tunnel type plasma reactive spraying [23] whose concept is shown in **Fig.36**. Using this method it is easy to obtain thick TiN coatings in a short time of 10 seconds.

Figure 37 shows the cross section of typical TiN coatings and the surface view of the coating and the substrate. In this case, the spraying conditions of the gas tunnel type plasma reactive spraying were P=25kW, L = 60 mm, and t =4.8 s. The color of the TiN coating is gold and the Vickers hardness was about Hv=2000.

For the further wide application of the plasma system, the development of a new type of smart plasma system: confront electrode type plasma jet has been examined. The new plasma system has the possibility of producing

Table 9 Design of Smart Plasma System for thermal processing.

	Control Object
1. Performance of Plasma Jet	
＊Power Sources	current, voltage
＊Flow rate control system	gas flow rate
2. Control of process materials	substrate, powder
3. Operating system	
Process precise control of time and spatial distribution	
Automatic control of thermal process	

new materials such as nano-carbon, nano-tubes, etc. Here in order to develop smart plasma processes, the precise control of plasma factors is the key to success, and the factors are shown in **Table 9**.

10. Conclusions

The following results were obtained during the application of the gas tunnel type plasma system developed.

(1) The gas tunnel type plasma system has high energy density and also high efficiency as compared to the conventional ones, and can be applied to various thermal processing problems.

(2) One typical application is plasma spraying of ceramics such as Al_2O_3 and ZrO_2. And the characteristics of these ceramic coatings were found to be superior to the conventional ones

(3) The ZrO_2 composite coating has graded functionality in terms of the hardness and porosity, and has the possibility of the development of high functionally graded TBC (thermal barrier coating).

(4) Pure tungsten coating without oxidation was obtained onto stainless steel substrates using the gas tunnel type plasma spraying method.

(5) Another application of gas tunnel type plasma is surface modification of metals. TiN films and coatings were formed in a very short time of 5 s.

The development of new types of smart plasma system, and application of high-energy plasma to other fields are now being studied by controlling the operating conditions, etc.

During last nine years, a variety of experimental set-ups have been constructed for the investigations of different types of quasi-stationary plasma dynamic accelerating systems.

(6) These systems are capable of generating high energy directional plasma flows of required composition (gas - and erosion discharges) over a large range of plasma parameters in different media (vacuum, gas at low and high pressures).

(7) So far, the following plasma accelerators have been realized:

a) Magnetoplasma Compressor type (MPC); MPC-Yu type; one stage Erosive Plasma Dynamic system (EPDS) and, in final stage of construction, two stage Quasi-Stationary High Current Plasma Accelerator (QHPA).

b) Plasma flow produced by MPC-CG was used to investigate plasma flow interaction with solid silicon surface. Different types of submicron structure have been obtained.

Acknowledgement

References

1) Y. Arata, and A. Kobayashi, *J. High Temp. Soc.* **11-3,** 1984, pp.124-131

2) Y. Arata, and A. Kobayashi, *J. A. P.*, **59-9,** 1986, pp.3038-3044

3). Y. Arata, and A. Kobayashi, *J. J. A. P.*, **25-11,** 1986,pp.1697-1701 (1986)

4) Y. Arata, A. Kobayashi, Y. Habara and S. Jing; Gas Tunnel Type Plasma Spraying, *Trans. of JWRI*, Vol.**15-2**, 1986, pp227-231.

5) Y. Arata, A. Kobayashi, and Y. Habara: Ceramic coatings produced by means of a gas tunnel type plasma jet, J. Applied Physics, **62**, 1987, pp.4884-4889.

6) R. Vassen, G. Kerkhoff, and D. Stoever, Development of a micromechanical life prediction model for plasma sprayed thermal barrier coatings. *Mater. Sci. Eng.*, A303, 2001, p. 100-109

7) D.N. Assanis; *Journal of Materials Processing Technology,* Vol. **4** (1989), p. 232.

8) T. M. Yonushonis; *Journal of Thermal Spray Technology,* Vol. **6**(1) (1997), p. 50.

9) P. Ramaswamy, S. Seetharamu, K.B.R.Varma, and K.J. Rao, Thermal shock charateristics of plasma sprayed mullite coatings, *J. Therm. Spray Technol.*, **7**(4), 1999, p. 497-505

10) T. Araya; *J. Weld. Soc. Jpn.*, Vol.**57-4**, 1988, pp.216-222.

11) Y. Arata, A. Kobayashi and Y. Habara; Formation of Alumina Coatings by Gas Tunnel Type Plasma Spraying (in Japanese), *J. High Temp. Soc.,* Vol.**13**, 1987, pp.116-124.

12) A. Kobayashi, S. Kurihara, Y. Habara, and Y. Arata; Relation between Deposit characteristics and ceramic coating Quality in Gas Tunnel Type plasma spraying (in Japanese), *J. Weld. Soc. Jpn.*, Vol.**8**, 1990,

pp.457-463.

13) A. Kobayashi; Property of an Alumina Coating Sprayed with a Gas Tunnel Plasma Spraying, *Proc. of ITSC* , 1992, pp.57-62.

14) A. Kobayashi : Characteristics of High Hardness Alumina Coating Formed by Gas Tunnel Plasma Spraying, J. Thermal Spray Tech. **5-3** (1996) 298-302

15) A. Kobayashi; Formation of High Hardness Zirconia Coatings by Gas Tunnel Type Plasma Spraying, *Surface and Coating Technology,* Vol.**90**, 1997, pp.197-202.

16) A. Kobayashi and T. Kitamura; High Hardness Zirconia Coating by Means of Gas Tunnel Type Plasma Spraying(in Japanese), *J. of IAPS*, Vol.**5**, 1997, pp.62-68.

17) A. Kobayashi, T. Kitamura: Effect of heat treatment on high-hardness zirconia coatings formed by gas tunnel type plasma spraying, *VACUUM*, Vol.**59-1** 2000, pp.194-202.

18) A. Kobayashi : Graded Functionality of Zirconia Composite Coatings by Gas Tunnel Type Plasma Spraying, *Advances in Applied Plasma Science* **3** (2001) 149-154.

19) A. Kobayashi, Adherence of zirconia composite coatings produced by gas tunnel-type plasma spraying, *VACUUM,* **73** (2004) 511-517.

20) H. Maier, J. Luthin, M. Balden, et. al**.**, Development of tungsten coated first wall and …, *J. of Nuclear Materials*, **307-311** (2002) 116-120.

21) A. Kobayashi, Tungsten Coating for Thermal Fusion Material Produced by Gas Tunnel Type Plasma Spraying, *Trans. of JWRI*, **37-2** (2008) 227-231.

22). A. Kobayashi : Surface Nitridation of Titanium Metals by Means of Gas Tunnel Type Plasma Jet, *J.Mater.Eng.& Performance* **5-3** (1996) 373-380.

23) A. Kobayashi : Formation of TiN Coating by Gas Tunnel Type Plasma Reactive Spraying, *Surface and Coating Technology*, **132** (2000) 152-157.

24) Morozov A I, *Sov. J. Plasma Phys.,* 1990, 16 69

25) J. Purić, I.P. Dojčinović V.M. Astashynski, M.M. Kuraica and B.M. Obradović, Electric and Thermodynamic Properties of Plasma Flows Created by Magnetoplasma Compressor, *Plasma Sources Sci. Technol.,* **13**, 2004, 74.

26) I.P. Dojčinović, M.M. Kuraica, B.M. Obradović, N. Cvetanović and J. Purić, Optimization of plasma flow parameters of the magnetoplasma compressor, *Plasma Sources Sci. Technol.,* **16**, 2007, 72.

27) J. Purić, I.P. Dojčinović V.M. Astashynski, M.M. Kuraica and B.M. Obradović, Electric and Thermodynamic Properties of Plasma Flows Created by Magnetoplasma Compressor, *Plasma Sources Sci. Technol.,* **13,** 2004, 74-84.

28) I.P. Dojcinovic, M.R. Gemisic, B.M. Obradovic, M.M. Kuraica, V.M. Astashinskii and J. Puric, Investigation of Plasma Parameters in a Magnetoplasma Compressor, *J.Appl. Spectroscopy,* **68,** 2001, 824-830

29) L. D. Landau and E. M. Lifshitz, *Fluid Mechanics, Pergamon Press, New York, 1987*

30) I.P. Dojčinović, M.M. Kuraica, B.M. Obradović and J. Purić, Silicon Surface Periodic Structures Produced by Plasma Flow Induced Capillary Waves, *Applied Physics Letters,* **89,** 2006, 071501.